# Supporting information

**Structure and mechanical properties of the ribosomal L1 stalk three-way junction**

K. Réblová, J. Šponer and F. Lankaš

## S1. Scatter plots, equilibrium conformations, and anisotropies

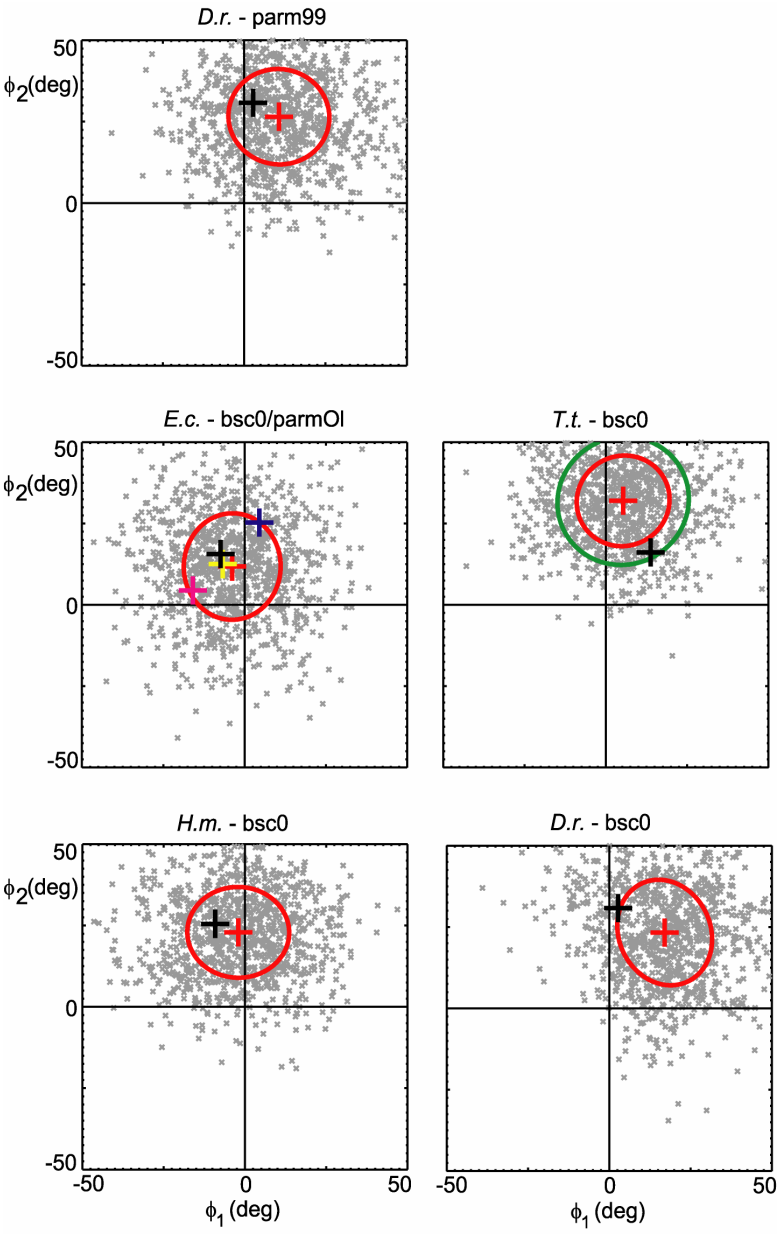


**Figure S1.** Scatter plots and energy contours for the global coordinates. The organism and the force field used are indicated ("bsc0" stands for the parmbsc0 force field). Meaning of symbols and colour coding is the same as in Fig. 3. The green ellipse is the energy contour corresponding to the energy of $k_B T$ .

**Table S1.** Conformations and anisotropies of the studied systems.

| | $\phi_1$ (deg) | $\phi_2$ (deg) | anisotropy |
|---|---|---|---|
| *E.c.* starting (2AWR) | -7 | 16 | - |
| *E.c.* equilibrium, parm99 | -9 | 13 | 1.1 |
| *E.c.* equilibrium, bsc0 | -4 | 12 | 1.1 |
| *E.c.* 2I2V | -7, *0*[*] | 13, *0* | - |
| *E.c.* 3I1N | -16, *-4* | 4, *2* | - |
| *E.c.* 3I1P | 5, *1* | 25, *-9* | - |
| *H.m.* starting (1S72) | -9 | 26 | - |
| *H.m.* equilibrium, parm99 | -3 | 20 | 1.1 |
| *H.m.* equilibrium, bsc0 | -2 | 23 | 1.1 |
| *T.t.* starting (1VSP) | 14 | 16 | - |
| *T.t.* equilibrium, parm99 | 4 | 23 | 1.1 |
| *T.t.* equilibrium, bsc0 | 5 | 32 | 1.0 |
| *D.r.* starting (1ZJR) | 3 | 31 | - |
| *D.r.* equilibrium, parm99 | 11 | 27 | 1.1 |
| *D.r.* equilibrium, bsc0 | 17 | 23 | 1.2 |
| *bulgeL*, equilibrium | 9 | 7 | 1.5 |
| *bulgeR*, equilibrium | 9 | 25 | 1.3 |

[*] Values in italics are from Fu et al. (ref. 18).

## S2. Anisotropic model of global structure and stiffness

We interpret the fluctuations of $\phi_1, \phi_2$ using a model in which the elastic energy is a general quadratic function of $\phi_1, \phi_2$:

$$\tilde{E}(\tilde{\boldsymbol{\omega}}) = \frac{1}{2}\left(\tilde{\boldsymbol{\omega}} - \hat{\tilde{\boldsymbol{\omega}}}\right) \cdot \tilde{\mathbf{K}} \left(\tilde{\boldsymbol{\omega}} - \hat{\tilde{\boldsymbol{\omega}}}\right) \tag{S1}$$

where $\tilde{\boldsymbol{\omega}} = (\phi_1, \phi_2)$ is the coordinate vector, $\hat{\tilde{\boldsymbol{\omega}}} = (\hat{\phi}_1, \hat{\phi}_2)$ is a vector of equilibrium shape parameters and $\tilde{\mathbf{K}}$ is a symmetric, positive definite stiffness matrix. Assuming the canonical probability distribution of the coordinates and small fluctuations, we deduce the relations between the model parameters and the moments of the coordinates (see refs 73-77):

$$\left\langle \tilde{\boldsymbol{\omega}} \right\rangle = \hat{\tilde{\boldsymbol{\omega}}}, \qquad \tilde{\mathbf{C}} = k_B T \tilde{\mathbf{K}} \tag{S2}$$

where $\left\langle \tilde{\boldsymbol{\omega}} \right\rangle$ is the mean and $\tilde{\mathbf{C}}$ the covariance matrix of the coordinate vector $\tilde{\boldsymbol{\omega}}$, $T$ is the absolute temperature and $k_B$ the Boltzmann constant. The model parameters $\hat{\tilde{\boldsymbol{\omega}}}$, $\tilde{\mathbf{K}}$ in general depend on the location of the segment within H76, that is, on the contour length $L$.

We now describe the more detailed model in which a homogeneous, straight elastic rod representing the helix H76 is attached to a flexible, spherical hinge representing the junction core. The model allows for the hinge and the rod to be anisotropically flexible. Consider a helical segment of H76 at a distance $L$ from the junction along the H76 contour. To describe the configuration of the model, we express the bending coordinates $\phi_1, \phi_2$ introduced above as a sum of two terms,

$$\begin{aligned} \phi_1 &= \phi_{J1} + \phi_{H1} \\ \phi_2 &= \phi_{J2} + \phi_{H2} \end{aligned} \tag{S3}$$

where $\phi_{J1}, \phi_{J2}$ are contributions to $\phi_1, \phi_2$ from the junction core and $\phi_{H1}, \phi_{H2}$ are contributions to $\phi_1, \phi_2$ from the helix H76 (see Fig. 4). The elastic energy is assumed to have the form

$$E = E_J + E_H \tag{S4}$$

where $E_J$ is a general quadratic function of $\phi_{J1}, \phi_{J2}$ and $E_H$ is a general quadratic function of $\phi_{H1}, \phi_{H2}$. Thus, the elastic energy is a sum of the contribution from the junction core and the contribution from the helix. For a given bending deformation, the elastic energy of a straight elastic rod is inversely proportional to its contour length (see e.g. ref. 97). From this and from eqn (S4) we deduce that our elastic energy $E$ takes the form

$$E(\boldsymbol{\omega}) = \tfrac{1}{2}(\boldsymbol{\omega} - \hat{\boldsymbol{\omega}}) \cdot \mathbf{K} (\boldsymbol{\omega} - \hat{\boldsymbol{\omega}}) \tag{S5}$$

where $\boldsymbol{\omega} = (\phi_{J1}, \phi_{J2}, \phi_{H1}, \phi_{H2})$ is the coordinate vector, $\hat{\boldsymbol{\omega}} = (\hat{\phi}_{J1}, \hat{\phi}_{J2}, \hat{\phi}_{H1}, \hat{\phi}_{H2})$ is a vector of equilibrium shape parameters and

$$\mathbf{K} = \begin{pmatrix} \mathbf{K}_J & 0 \\ 0 & (1/L)\mathbf{K}_H \end{pmatrix} \tag{S6}$$

is a symmetric, positive definite, block-diagonal stiffness matrix, whose diagonal blocks $\mathbf{K}_J$ and $(1/L)\mathbf{K}_H$ are stiffness matrices associated with the junction core and with the helix, respectively. The assumption of the helix being straight implies that

$$\hat{\phi}_{H1} = \hat{\phi}_{H2} = 0 \tag{S7}$$

Assuming the canonical probability distribution for the coordinates and small fluctuations, we find the moment-parameter relations

$$\langle \boldsymbol{\omega} \rangle = \hat{\boldsymbol{\omega}}, \qquad \mathbf{C} = k_B T \mathbf{K}^{-1} \tag{S8}$$

where $\langle \boldsymbol{\omega} \rangle$ is the expected value and $\mathbf{C}$ the covariance matrix of the coordinate vector $\boldsymbol{\omega}$. From this and from the block-diagonal form of the stiffness matrix we obtain the relation

$$\mathbf{C} = k_B T \begin{pmatrix} \mathbf{K}_J^{-1} & 0 \\ 0 & L\mathbf{K}_H^{-1} \end{pmatrix} \tag{S9}$$

Thus, the covariance matrix of $\boldsymbol{\omega}$ is block diagonal. Its diagonal blocks are the covariance matrices of $\phi_{J1}, \phi_{J2}$ and $\phi_{H1}, \phi_{H2}$ respectively and are given by

$$\mathbf{C}_J = k_B T \mathbf{K}_J^{-1}, \qquad \mathbf{C}_H = k_B T L \mathbf{K}_H^{-1} \tag{S10}$$

The coordinates $\phi_{J1}, \phi_{J2}$ and $\phi_{H1}, \phi_{H2}$ are not directly accessible to measurement, since our helix segments are of finite length and thus we cannot make $L$ arbitrarily small. Rather, we measure only the values of $\phi_1, \phi_2$. From eqn (S8), (S7) and (S3) we get

$$\langle \phi_1 \rangle = \hat{\phi}_{J1}, \qquad \langle \phi_2 \rangle = \hat{\phi}_{J2} \tag{S11}$$

This shows that the mean values of $\phi_1, \phi_2$ are independent of $L$ and equal to the equilibrium coordinates of the junction core.

From the block-diagonal form of $\mathbf{C}$ and from eqn (S3) we deduce that the covariance matrix $\tilde{\mathbf{C}}$ for $\phi_1, \phi_2$ has the form

$$\tilde{\mathbf{C}} = \mathbf{C}_J + \mathbf{C}_H \tag{S12}$$

Substituting from eqn (S10) to the right-hand side of eqn (S12), we obtain

$$\tilde{\mathbf{C}} = k_B T(\mathbf{K}_J^{-1} + L\mathbf{K}_H^{-1}) \qquad \text{(S13)}$$

Hence, the matrix elements of $\tilde{\mathbf{C}}$ are linear functions of the contour length $L$. The absolute term is the covariance matrix of the junction core coordinates $\phi_{J1}, \phi_{J2}$ and is related to the stiffness of the junction core through eqn (S10a). The linear term is the covariance matrix of the helix coordinates $\phi_{H1}, \phi_{H2}$ and is related to the stiffness of the helix through eqn (S10b).

The model simplifies further if the junction core and the helix are assumed isotropically flexible. In that case the stiffness matrices have the form

$$\mathbf{K}_J = a_J \mathbf{I}, \qquad \mathbf{K}_H = a_H \mathbf{I} \qquad \text{(S14)}$$

where $a_H > 0, a_J > 0$ are the stiffness constants and $\mathbf{I}$ is the identity matrix. From eqn (S14) and (S13) we obtain that the covariance matrix $\tilde{\mathbf{C}}$ of the isotropic model takes the form

$$\tilde{\mathbf{C}} = k_B T\left(\frac{1}{a_J} + \frac{L}{a_H}\right)\mathbf{I} \qquad \text{(S15)}$$

that is, $\tilde{\mathbf{C}}$ is a diagonal, isotropic matrix whose entries are linear functions of the contour length $L$.

Eqn (S15) can be given a simple interpretation. We define the total square angular deviation $(\Delta\phi)^2$ as

$$\Delta\phi^2 = \left(\phi_1 - \hat{\phi}_1\right)^2 + \left(\phi_2 - \hat{\phi}_2\right)^2 \qquad \text{(S16)}$$

and the square angular deviations associated with the junction core and with the helix as

$$\left(\Delta\phi_J\right)^2 = (\phi_{J1} - \hat{\phi}_{J1})^2 + (\phi_{J2} - \hat{\phi}_{J2})^2, \quad \left(\Delta\phi_H\right)^2 = (\phi_{H1} - \hat{\phi}_{H1})^2 + (\phi_{H2} - \hat{\phi}_{H2})^2 \qquad \text{(S17)}$$

Taking the trace of both sides of eqn (S12) and using eqn (S2a) and (S8), we find

$$\left\langle \Delta\phi^2 \right\rangle = \left\langle \left(\Delta\phi_J\right)^2 \right\rangle + \left\langle \left(\Delta\phi_H\right)^2 \right\rangle \qquad \text{(S18)}$$

We then substitute eqn (S14) to eqn (S10) and compute the trace of both sides, which gives

$$\left\langle \left(\Delta\phi_J\right)^2 \right\rangle = 2k_B T / a_J, \qquad \left\langle \left(\Delta\phi_H\right)^2 \right\rangle = 2k_B L / a_H \qquad \text{(S19)}$$

From eqn (S18) and (S19) we finally obtain that

$$\left\langle \Delta\phi^2 \right\rangle = 2k_B T\left(\frac{1}{a_J} + \frac{L}{a_H}\right) \qquad \text{(S20)}$$

Thus, in the isotropic model, the bending angle variation $\langle \Delta\phi^2 \rangle$ is a linear function of the contour length $L$. The absolute term is the angular variation $\langle (\Delta\phi_J)^2 \rangle$ associated with the junction core, related to the junction core stiffness constant $a_J$ by eqn (S19a). The linear term is the angular variation $\langle (\Delta\phi_H)^2 \rangle$ associated with the helix, related to the helix stiffness constant $a_H$ by eqn (S19b).

**Fitting of the model**

We extracted the time series of the coordinates $\phi_1, \phi_2$ from the MD trajectories as described in the main text. We then estimated the mean and covariance of $\phi_1, \phi_2$ over the canonical ensemble by their mean and covariance over the MD time series. As shown above, the model predicts the covariance matrix $\tilde{\mathbf{C}}$ to be a linear function of the contour length $L$. To verify this prediction, we computed the matrix elements of $\tilde{\mathbf{C}}$ for various values of $L$. This was done for the *E.c.*, *H.m.* and *T.t.* simulations and each time for the two force field choices, that is, for six systems in total. The *D.r.* simulations were excluded due to instabilities at the bottom of H76.

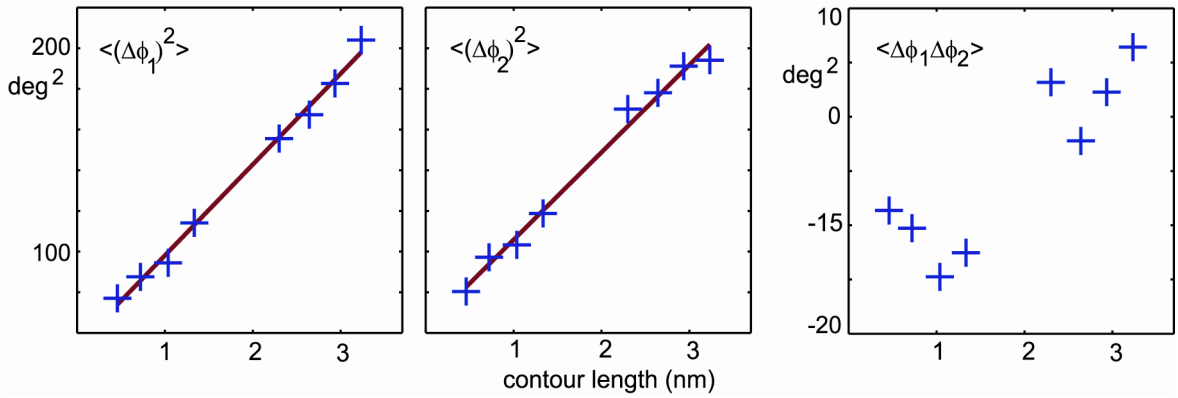


**Figure S2.** Matrix elements of $\tilde{\mathbf{C}}$, the covariance matrix of the coordinates $\phi_1, \phi_2$, as a function of the contour length $L$. These data are for the *T.t.*/parmbsc0 simulation, all the other cases are similar.

All the plots show a similar pattern (Fig. S2): the diagonal entries of $\tilde{\mathbf{C}}$ are very close to linear in $L$, the off-diagonal entries are not linear but they are small, 5-10 times smaller than the diagonal entries. Thus, the covariance matrix is close to diagonal. We therefore set the off-diagonal entries of $\tilde{\mathbf{C}}$ to zero and computed the stiffness parameters from the linear fit to the diagonal entries using eqn (S13). We found that the junction core stiffness matrix $\mathbf{K}_J$ and the helix stiffness matrix $\mathbf{K}_H$ (or equivalently, the covariance matrices $\mathbf{C}_J$ and $\mathbf{C}_H$) are nearly isotropic. Just as in the main text, we define anisotropy of a covariance matrix as the square root of its eigenvalues (since $\mathbf{C}_J$ and $\mathbf{C}_H$ are diagonal, their eigenvalues are equal to their diagonal entries). Anisotropies of the junction core as well as of the helix, for all the six systems, do not exceed 1.2. This indicates that the data are well described by the isotropic model expressed by eqn (S19), (S20).

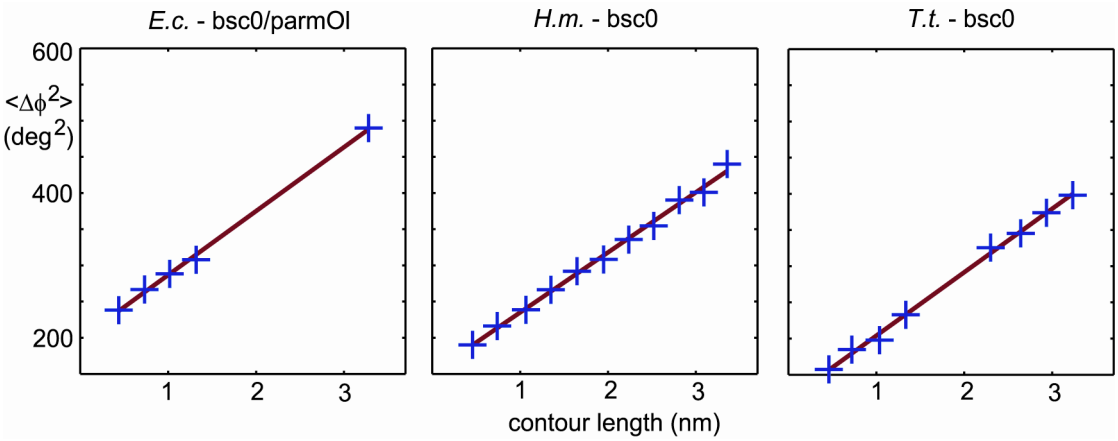


**Figure S3.** Bending angle variation as a function of the contour length. Meaning of symbols is the same as in Fig. 4.

## S3. Structure stability and interatomic contacts

### Structure stability

In the simulations of *E.c.*, *T.t.* and *H.m.*, we observed frequent fluctuations and opening events for canonical and wobble base pairs forming the helices. In both parm99 and parmbsc0 simulations of *D.r.*, we observed large fluctuations in the two wobble pairs at the base of H76 (G2077/U2178 and G2078/U2176) – for most of the simulation time, the pairs were stabilized just by a single H-bond. Another perturbation was seen in the adjacent canonical base pair (A2079-U2175), which often adopted a non-planar geometry. These three pairs are not perfectly structured in the initial x-ray structure, which probably affected their behavior during simulations. The central tH/S A/G and tH/W A/U pairs (Fig. 2) forming the UNA/GAN motif and simultaneously the hook-turn were stable in both parm99 and parmbsc0 simulations. The third non-canonical single hydrogen bonded tH/H pair either fluctuated or it was disrupted.

We observed a substantial increase in the interphosphate distances over major groove in our simulated structures compared to the corresponding x-ray structures (Fig. S5). The increase was typically 7 Å for parm99 and 6 Å for parmbsc0 simulations. Further investigation of the phenomena and its relationship to the local conformation of the helices is a subject of an ongoing study. The x-ray *T.t.* 3wj conformation is affected by its interaction with the E-site tRNA, which causes a compression of major groove in the upper part of H76 (19). During the first nanoseconds of *T.t.* simulations the compressed major groove opened and remained in this new geometry for the whole simulation.

### Bulge dynamics

*BulgeL*: In the time period of 0-60 ns, the bulge base stayed in the starting stacked-in conformation and temporarily paired with opposite uracil from the adjacent lower A-U base pair. In the time period of 60-100 ns, the bulge base formed a triplet with the adjacent upper G=C base pair.

*BulgeR*: After equilibration, the bulge base formed a triplet with the adjacent lower A-U base pair. This conformation was stable until 58 ns, when the A-U pair was disrupted and the uracil flipped out of the stem. The bulge base was then forming a non-canonical A/A pair with the remaining adenine for 10 ns. After that the A/A pair broke and the bulge base flipped out of the stem, which did not change until the end of the simulation.

**Contacts in the central part of the 3wj**

The x-ray structures of most of the studied systems contain two sugar-phosphate contacts in the central part (the first one between 2'-OH of the uracil from the tH/H pair and a phosphate of the adjacent nucleotide from H75, the second one between a phosphate of the uracil from the tH/H and 2'-OH of the adenine from the tH/S pair (Fig. S4 and Table S1). These contacts were maintained in the majority of the simulations, their stability is indicated in Table S1. In addition, the *H.m.* 3wj exhibits a base-base contact between the bulge cytosine 2259 and the adenine from the tH/S pair, C2259(N4)-A2244(N1) (Fig. S3 and S4). The corresponding contacts are not seen in *E.c.*, *T.t.* and *D.r.* x-ray structures (probably due to their lower resolution); nevertheless, they were formed during the simulations (Table S1).

Further, the *H.m.* structure also shows a base-phosphate contact, classified as 7BPh, between the cytosine of the first pair of H79 and the adjacent adenine from the tH/S pair, C2245(N4)-A2244(O2P), and a base-sugar contact between the guanine of the tH/S pair and the bulge cytosine from the junction core, C2243(O2')-G2257(N2). The first contact broke at the beginning of both parm99 and parmbsc0 simulations and the second contact was replaced with the C2243(O2')-G2257(N1) contact in both parm99 and parmbsc0 simulations. *T.t.* 3wj also shows a base-sugar contact between the guanine of the tH/S pair and the uracil of the tH/W pair, U2197(O2')-G2224(N1). This contact was stable in both parm99 and parmbsc0 simulations. In both *D.r.* simulations, we detected a new (not seen in x-ray) and stable base-phosphate interaction (class 4BPh) between the bulge adenine A2181 and the guanine from the tH/S pair, A2181(O2P)-2204G(N1/N2). A new stable contact was also seen in both *E.c.* simulations, namely between the guanine from the tH/S pair and the uracil from the tH/W pair, G2224(N1)-U2197(O2').

In summary, the central region in all the four studied structures is interconnected by four stable contacts: three of them are indicated in Fig. S1 and Table S1, the fourth one is different in each system, but it always involves the guanine from the tH/S base pair.

**Contacts of H75 and H79 to the rest of the ribosome**

In the x-ray structures, H75 and H79 create a number of contacts with the surrounding structure. In particular, H75 and H79 of *T.t.* 3wj exhibit contacts with ribosomal proteins L2 and L28P. The first two base pairs of *T.t.* H76 (2093G=C2196 and 2097G=2195C) and the central part of *T.t.* junction also have several contacts with ribosomal protein L9 (Fig. S6A, B). In addition, H75 makes contacts with H68 and H21, and H79 makes contacts with H66 and H58.

The *E.c.* structure shows similar contacts with L2 and L9 proteins as the *T.t.* structure, but specific direct contacts between L9 and first two base pairs of H76 are not seen. The L28P is replaced in the *E.c.* structure by L31 and makes contacts to both H75 and H79 (data not

shown). The RNA-RNA contacts are also similar, but not identical, to the *T.t.* structure: H75 makes contacts to H68 and H21, H79 makes contacts with H66, H58 and also with H52, which is not seen in the *T.t.* structure.

In the *D.r.* structure there are contacts of H75 and H79 only with L2 and L28 proteins, the L9 protein is missing. The RNA-RNA contacts in the *D.r.* structure are similar to *E.c.* and *T.t.* structures: H75 makes contacts to H68, H21 and H66, and H79 makes contacts to H52 and H58.

In the *H.m.* structure, both H75 and H79 make contacts with L2P, which corresponds to L2 in the eubacterial structures. In addition, the central part of the junction and H75 make contacts to L15E instead of to L28, the L9 protein is missing. The RNA-RNA contacts are less extensive compared to eubacterial structures (the H75 makes contacts to H68 and H21, and H79 makes contacts only to H66).

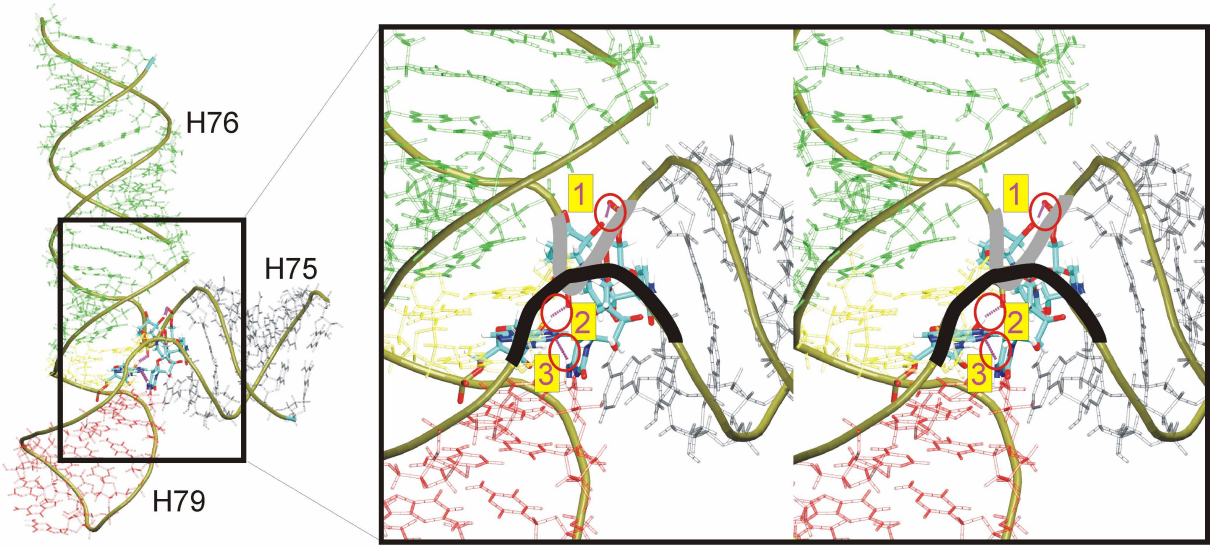


**Figure S4.** Left: the x-ray structure of *H.m.* 3wj. H76 is green, H75 is blue and H79 is red, the tH/S and tH/W pairs, including the bulge base between them, are in yellow. Right: a stereo view showing details of the central region with the sugar-phosphate contacts 2132C(O2P)-2133U(O2') and 2133U(O1P)-2244A(O2') (1 and 2, in red circles) and a base-base contact (2244A(N1)-2259C(N4) (3, in a red circle). The two bends of the sugar phosphate backbone at the H76/H79-H75 interface are in black (H75 to H79) and in grey (H75 to H76).

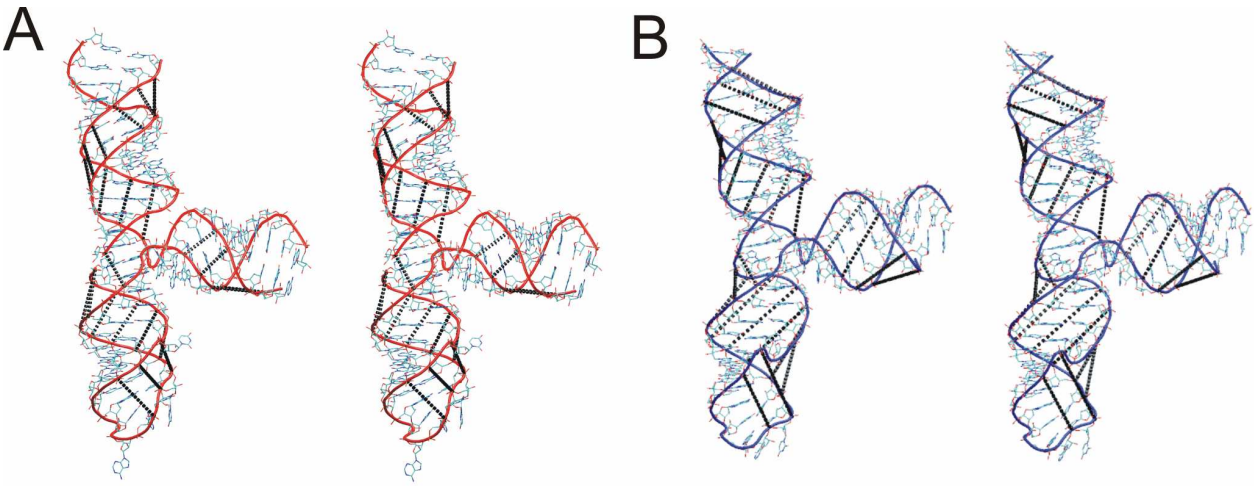


**Figure S5.** Stereo views of the x-ray *E.c.* 3wj (A) and the MD structure from parm99 simulation averaged over the last 10 ns (B). Interphosphate distances are highlighted. Notice the considerable increase of the distances in the MD structure compared to the x-ray structure.

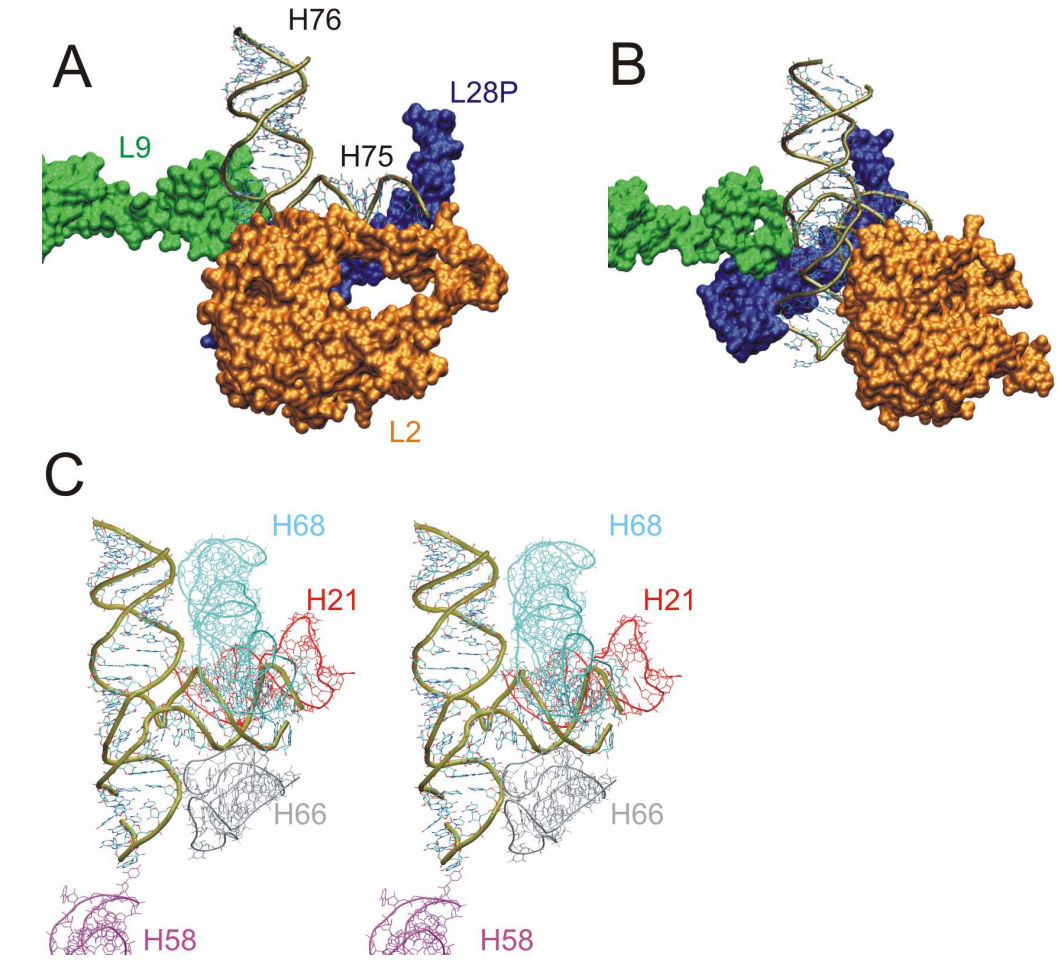


**Figure S6.** Interactions of *T.t.* 3wj with ribosomal proteins (A: front view, B: side view) and with the surrounding RNA helices (C: stereo view).

**Table S2.** Occurrence of the two main base-phosphate and one base-sugar contacts[#] at the H76/H79-H75 interface in the x-ray structures and their stability[*] in the simulations.

| Organism (pdb code) | Contact 1[#] | Contact 2[#] | Contact 3[#] |
|---|---|---|---|
| *D.r.* (2ZJR) | 2074U(O2P)-2075U(O2')<br>parm99: 80%<br>parmbsc0: 100% | [x] 2075U(O2P)-2182A(O2')<br>parm99:100%<br>parmbsc0: 95% | 2182A(N1)-2205C(N4)<br>parm99:100%<br>parmbsc0: 100% |
| *E.c.* (2AW4) | [x] 2091C(O2P)-2092U(O2')<br>parm99: 100%<br>parmbsc0_parmOl: 100% | [x] 2092U(O1P)-2199A(O2')<br>parm99: 98%<br>parmbsc0_parmOl: 75% | 2199A(N1)-2226C(N4)<br>parm99:65%<br>parmbsc0_parmOl: 90% |
| *H.m.* (1S72) | [x] 2132C(O2P)-2133U(O2')<br>parm99: 100%<br>parmbsc0: 100% | [x] 2133U(O1P)-2244A(O2')<br>parm99: 100%<br>parmbsc0: 65% | [x] 2244A(N1)-2259C(N4)<br>parm99: 100%<br>parmbsc0: 65% |
| *T.t.* (1VSP) | [x] 2091U(O2P)-2092U(O2')<br>parm99: 98%<br>parmbsc0: 100% | [x] 2092U(O1P)-2199A(O2')<br>parm99: 100%<br>parmbsc0: 95% | 2199A(N1)-2226C(N4)<br>parm99: 40%<br>parmbsc0: 100% |

[#] Positions of these contacts are shown in Fig. S4.
[*] Stability of contacts in parm99 and parmbsc0 simulations is indicated in percentage. For the *E.c.* system we used parmbsc0 force field together with the parm$\chi$Ol$_3$ correction (see Methods).
[x] Contact seen in the initial x-ray structure.